Automatic Segmentation of Lower-Limb Arteries on CTA for Pre-surgical Planning of Peripheral Artery Disease

Lisa Guzzi[1,2,3], Maria A. Zuluaga[2], Fabien Lareyre[4,5], Gilles Di Lorenzo[4], Sébastien Goffart[1,3], Andrea Chierici[3], Juliette Raffort[3,5], and Hervé Delingette[1]

[1] Université Côte d'Azur, Inria, Epione Team, Sophia Antipolis, France
[2] Data Science Department, EURECOM, Sophia Antipolis, France
[3] University Hospital of Nice, Nice, France
[4] Department of Vascular Surgery, Hospital of Antibes Juan-les-Pins, Antibes, France
[5] Université Côte d'Azur, CNRS, UMR7370, LP2M, Nice, France
lisa.guzzi@inria.fr

Abstract. Peripheral artery disease (PAD) often requires revascularization guided by computed tomography angiography (CTA). Manual analysis of lower-limb arteries on CTA is time-consuming, operator-dependent, and limited by challenging imaging conditions. While deep learning has advanced vascular segmentation, current models focus on large central vessels and do not capture the full arterial anatomy and pathological conditions in the lower extremities for PAD. In this work, we present a fully automated 3D segmentation pipeline tailored to PAD to delineate the entire lower-limb arterial tree, including the recognition of each main and peripheral branches, along with calcified plaques and stents. Our framework leverages nnU-Net, and addresses the limitations in complex PAD settings by introducing (1) a PAD-specific annotation protocol using a semi-automated tool to reduce inter-observer variability in labeling stents and calcifications, (2) a novel object-level detection metric that accounts for boundary ambiguity in calcified lesions and stents, and (3) the incorporation of the clDice loss to enhance topological preservation, critical for vascular analysis in a pathological setting. We train and evaluate our method on a curated in-house dataset under challenging imaging conditions. Our pipeline demonstrates robust performance, enabling the extraction of clinically relevant features necessary to the pre-surgical planning. It paves the way for fully automated PAD assessment, with potential to improve diagnostic accuracy, reduce time to treatment, and more objective severity scoring for therapy planning.

Keywords: Peripheral Artery Disease · Computed Tomography Angiography · Image Segmentation.

1 Introduction

Peripheral artery disease (PAD) is a common atherosclerotic condition affecting an estimated quarter billion people worldwide [10, 12, 17]. It carries high mor-

bidity and mortality and often presents as chronic limb threatening ischemia requiring revascularization [5, 7, 8]. Computed tomography angiography (CTA) is widely used in this context as vascular surgeons rely on precise 3D visualization of arterial anatomy and lesion characteristic to plan intervention [4]. The extent and location of occlusions or stenosis, calcifications and prior stents as well as the general artery anatomy of the patient strongly influence the revascularization strategy [12]. However, manual analysis of lower extremity CTA is time-consuming and operator-dependent. Thus, the automatic segmentation of the lower-limb arteries, along with detection of calcified plaque and stents, could greatly accelerate pre-surgical planning. The automatic measurements could help retrieving useful informations for example to calculate standardized staging scores (such as GLASS [18] or the TASCII score [13]) from the imaging, supporting personalized therapy. However, PAD presents unique segmentation challenges: arteries are often narrowed or occluded, distal branches can be small and tortuous, and heavy calcifications and surgical stents cause imaging artifacts, degrading conventional segmentation performance. Vessel segmentation networks may falsely break vessels at occlusions or bleed into high-contrast plaque. Clinically, missing a side branch or mis-measuring a lesion can misguide revascularization decisions.

Deep learning techniques for 3D image segmentation have advanced rapidly [1, 15]. It has been successfully used to segment different artery types and calcification plaques [6, 2, 11]. The nnU-Net framework [9] has emerged more recently as a self-configuring state-of-the-art method for medical image segmentation. It was used for example to segment carotid arteries and calcified plaques on CTA [20]. Zhou et al. [14] additionally proposed a general CTA model for multiple anatomical structures and lesions, and outperformed prior methods on all evaluated structures using the nnU-Net framework, notably including coronary arteries, aorta, and lower limb arteries. While these studies show the potential of deep learning to segment vascular structures on CTA, most focus on major vessels such as the aorta, coronaries, carotids or on classification tasks, but none of them fully segment the total lower-limb arterial tree, typically stopping at the iliac or femoral level. To further improve the segmentation of fine tubular structures, the clDice loss function [16] has been proposed. This loss explicitly enforces the overlap of predicted and ground-truth centerlines and preserves vessel topology. To our knowledge, these advances have yet to be fully exploited for the entire lower limb vasculature in PAD patients.

In this study, we address these gaps by applying a fully automatic 3D segmentation pipeline in a clinically realistic PAD population on CTA imaging. Building upon the nnU-Net framework, we train on a curated in-house annotated CTA volumes to segment the entire lower-limb arterial tree, including major named vessels, secondary branches, calcified plaques, and implanted stents. Beyond standard segmentation, we tackle several PAD-specific challenges. First, the complex morphology and variable imaging appearance of calcifications and stents on CTA introduce significant ambiguity in manual annotations. To mitigate inter-annotator variability, we developed a semi-automatic labeling tool tailored to these structures. Second, conventional voxel-based metrics often under-

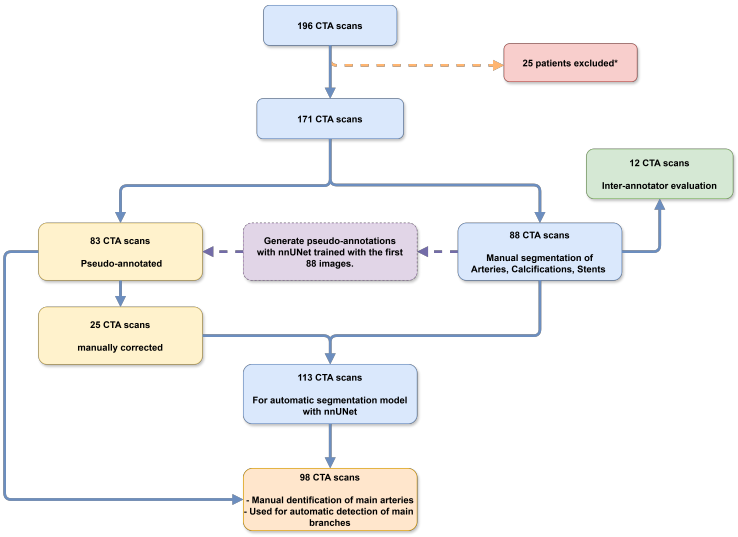

Fig. 1: Flowchart of the Dataset distribution in each task.

estimate performance when boundary definitions are uncertain for small objects, we therefore introduce an object-level detection metric designed to faithfully reflect the detection of calcified plaques and stents. Third, to ensure continuity and topological integrity of the segmented vessels, crucial for downstream clinical analysis, we incorporate the clDice loss alongside Dice and Cross-Entropy (CE) during training. Compared to prior work, each arterial segment is explicitly labeled, enabling the extraction of region-specific features such as local calcification burden or anatomical variants. It supports detailed preoperative planning, facilitates reproducible quantification of disease severity, and lays the foundation for automated stenosis and thrombosis assessment in PAD.

2 Method

2.1 Dataset

For this study, a dataset of 196 lower-limb Computed Tomography Angiography (CTA) anonymized scans from patients with Peripheral Artery Disease (PAD) was acquired from the Hospital of Nice, following the French Regulatory Health Authorities, and with informed consent from all subjects. A total of 25 scans were excluded due to suboptimal image quality, including issues related to anatomical coverage, resolution or when the contrast product was not visible in the arteries. The remaining 171 scans were converted from DICOM to NIfTI format, resulting in 3D volumes with a mean image dimension of 512 x 512 x 1657 slices ($\pm$ 595) and a mean voxel spacing of 0.81 x 0.81 x 0.77 mm ($\pm$ 0.11 $\times$ 0.11 $\times$ 0.83 mm).

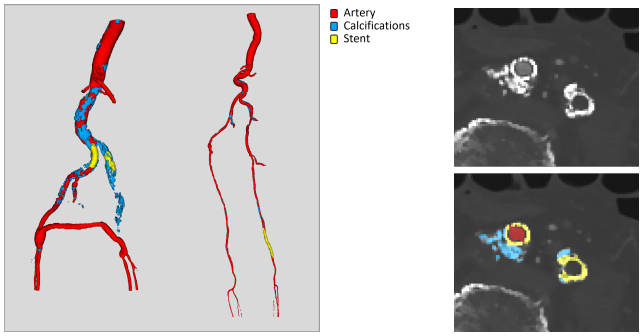

(a) (b)

Fig. 2: (a) A 3D representation of Artery, Calcification and Stent segmentation. (b) Axial CTA representation with and without segmentation annotations.

2.2 Annotation protocol

From the 171 selected CTA scans, 88 were randomly selected for manual segmentation. This manual segmentation was performed by two experts based on a consensus, and inter-annotator variability was assessed on a subset of 12 scans independently annotated by the two experts. The segmented structures include the arteries, calcification plaques, and stents (Fig. 2). Segmentation was performed using ITK-SNAP v4.0 [19] with an adaptive brush tool based on the watershed algorithm. The arterial tree was annotated in the axial plane, beginning at the abdominal aorta until the fibular and tibial arteries. Collateral arteries and secondary branches were segmented up to their first bifurcation or until they became indistinguishable.

Inter-annotator evaluation. The inter-annotator agreement on the 12 independently labeled scans for the global arterial tree achieved a Dice score of 0.91, indicating strong overall concordance. However, agreement was lower for distal branches in the below-knee region (Dice: 0.40), compared to the Aorto-Iliac (Dice: 0.94) and Femoral-Popliteal (Dice:0.88) regions, reflecting greater variability in segmenting small-caliber vessels. This reduced agreement is attributed to the sensitivity of the Dice metric to minor boundary differences in small structures. Final ground truth segmentations were therefore derived from a consensus of the two experts. For calcifications and stents, inter-annotator agreement was substantially lower, with a Dice of 0.42 for the calcifications and 0.41 for the Stents. This is primarily due to the small size of these structures and the inherent difficulty in visually identifying their exact boundaries on CTA. It highlights the subjectivity and variability of manual annotation for such small targets.

Semi-automatic labeling. Due to the difficulty in manually defining the exact boundaries of calcifications and stents, we propose a semi-automatic tool to

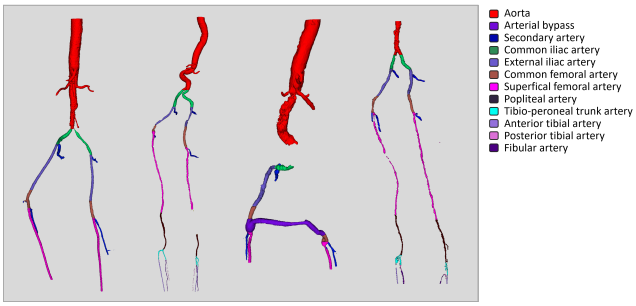

Fig. 3: 3D representation of main branches of the arteries of the lower limbs.

reduce operator bias and improve annotation consistency. Gaussian clustering was applied to the intensity distribution of voxels adjacent to the artery mask. The cluster of voxels with Hounsfield Unit (HU) values above 700 was initially classified as calcifications. Due to overlapping intensity ranges, stents and bones were manually distinguished and corrected post-clustering.

Final label processing. Each segmentation underwent further refinement by removing small connected components (< 5 voxels) and applying the Tukey interquartile range method to clip outlier intensities. After the initial manual segmentations, a preliminary nnU-Net model was trained on the 88 labeled images and applied to 25 additional unlabeled scans. These pseudo-labels were manually corrected to increase the sample size to 113 annotated scans.

Branch annotation. A second segmentation protocol was implemented to label individual arterial segments on 98 scans, specifically to differentiate main artery branches, secondary branches and bypass arteries (Fig. 3). An expert provided proximal and distal landmarks for each branch over the artery mask, including the aorta, common iliac artery, external iliac artery, superficial femoral artery, popliteal artery, tibial artery, posterior tibial artery, fibular artery and tibio peroneal trunk. All other segments were categorized as secondary branches. A semi-automatic labeling script connected annotated landmarks along the centerline of the artery mask to assign unique labels to each arterial segment. Manual corrections were subsequently applied to refine these labels.

2.3 Automatic segmentation

The automatic segmentation was performed using the nnU-net [1]. This framework is a self-configuring deep learning architecture designed for biomedical image segmentation. It automatically determines the model parameters based on the dataset's properties, including pre and post processing steps, training parameters, data augmentation techniques and the network architecture. The training of the segmentation framework was conducted in a 5 fold cross validation setup,

and then inferred and evaluated on a separate test set. For the final artery segmentation, scans were divided into 76 scans for the training, 20 scans for validation and 17 scans for the independent test set. The intensity normalization was automatically applied by nnU-Net, foreground voxel intensities from all training images were collected to compute the 0.5th and 99.5th percentiles. Voxel intensities were clipped to this range, followed by z-score normalization. Patch size was set to 96 × 320 × 80 voxels, voxel spacing was resampled to 0.838 × 0.62 × 0.828 mm, the training was performed with Adam optimizer and an initial learning rate of 0.01. The network configuration was empirically set to 3D network with full resolution of the image (3d_fullres). For the loss Function, the default nnU-Net uses a combination of CE and Dice loss. In addition, we investigated the use of clDice loss, which enhances topological preservation in tubular structures:

$$\mathcal{L}_{CE+Dice+clDice} = \lambda_1 \times \mathcal{L}_{CE} + \lambda_2 \times \mathcal{L}_{Dice} + \lambda_3 \times \mathcal{L}_{clDice} \quad (1)$$

where λ is a weighting factor controlling the contribution of the clDice term. In this training, the values of λ_1, λ_2, λ_3 were set respectively to 2, 1, 1.

Branch segmentation was performed similarly with nnU-Net. We divided the 98 annotated scans into 63 training, 16 validation and 19 scans for the independent test set. The branches each correspond to a submask of the global artery mask. Here the task is considered as a multi-label segmentation directly extracted from the CTA. Training was conducted on Nvidia A40 PCIe GPUs.

2.4 Evaluation metrics

Overlap-based metrics. We evaluated the predictions using the Dice score, the Precision, Recall, the Hausdorff Distance (HD) and its (HD95).

Topological-based metrics. These metrics assess the preservation of anatomical continuity and connectivity, which are crucial in vascular segmentation. The **clDice** [16] metric extends the traditional Dice metric by emphasizing the alignment of tubular structures along their centerlines. To evaluate topological consistency, we computed the mean absolute difference of **Betti numbers** where β_0, β_1 and β_2 respectively represent the number of connected components, loops, and cavities. Additionally, the **Euler characteristic** χ is defined as: $\chi = \beta_0 - \beta_1 + \beta_2$. We used a connectivity of 26 in the foreground and of 6 in the background.

Detection metrics. The segmentation of calcifications and stents presents a unique challenge due to their small size and the inherent subjectivity in delineating their exact boundaries. As a result, traditional voxel-wise metrics such as the Dice score can be overly sensitive to minor discrepancies. In clinical applications, the primary objective is to reliably detect the presence and approximate extent of each calcification or stent, rather than achieving perfect boundary accuracy. To assess detection performance, we employed an object-level matching

Table 1: nnU-Net segmentation performance of the global artery mask with and without incorporating the clDice loss, and segmentation of each arterial branch.

	Dice ↑	**clDice ↑**	**HD ↓**	**HD95 ↓**	**Prec. ↑**	**Rec. ↑**	$\beta_0 \downarrow$	$\beta_1 \downarrow$	$\beta_2 \downarrow$	$\chi \downarrow$
-	0.93	0.86	103.36	5.59	**0.93**	0.93	35.06	67.00	25.29	69.00
+ **clDice**	**0.94**	**0.88**	**93.42**	**3.43**	**0.93**	**0.95**	**24.65**	**59.53**	**22.12**	**54.29**
Aorta	0.96	0.90	402.78	2.85	0.97	0.94	3.85	8.65	6.89	6.20
Second.	0.68	0.61	245.90	52.00	0.75	0.65	5.58	0.85	0.30	5.55
C. iliac	0.79	0.84	28.93	13.05	0.81	0.81	0.60	1.25	1.05	1.10
E. iliac	0.79	0.87	39.25	11.43	0.83	0.79	1.50	1.75	0.30	2.05
C. fem.	0.67	0.72	78.29	63.69	0.71	0.69	1.10	0.45	0.05	1.50
S. fem.	0.75	0.78	156.49	48.16	0.78	0.76	7.80	3.25	1.50	7.15
Popliteal	0.49	0.62	169.40	111.10	0.74	0.40	2.27	0.47	0.06	2.06
TPT	0.45	0.60	35.45	29.02	0.79	0.33	1.53	0.12	0.06	1.47
A. Tib.	0.70	0.80	95.92	21.24	0.88	0.60	3.47	0.36	0.00	3.35
P. Tib.	0.32	0.55	73.15	33.92	0.97	0.20	32.70	0.18	0.06	32.83
Fibular	0.63	0.75	70.45	50.33	0.81	0.54	6.23	0.06	0.00	6.30

detection algorithm that compares individual segmented components between the ground truth and predicted segmentation masks. All connected components are extracted from both the ground truth and predicted segmentations. An object from the predicted segmentation is matched to a ground truth object if they share at least one voxel. In cases where multiple objects from one segmentation overlap with the same object in the other segmentation, those objects are merged into a single group to avoid redundant matches. For each matched object pair or group, the volumetric overlap is computed. An object is considered successfully detected if it overlaps by at least 30% (set empirically) with its corresponding ground truth object. This approach yields object-level counts of true positives (TP), false positives (FP), and false negatives (FN). Using these counts, we compute detection precision and recall, using the same formulas as voxel-based metrics but applied to objects rather than voxels. To distinguish them, we denote these metrics as **D_Pre** and **D_Rec**. The **F1 Score** is the harmonic mean of precision and recall and gives a balanced measure of segmentation accuracy.

3 Results

3.1 Automatic segmentation of the vascular system

The performance of the nnU-Net-based artery segmentation is summarized in Table 1. Combining the clDice loss with the Dice and CE losses consistently improved all metrics, achieving a final Dice score of 0.94 and clDice of 0.88. For the Branch-wise labeling, segmentation accuracy was higher for large, proximal arteries (in the iliac and femoral segments) and declined for smaller distal branches, particularly below the knee. These results mirror the results observed in inter-annotator agreement for these regions, suggesting that anatomical complexity and reduced label consistency negatively impacted the model learning.

Table 2: nnU-Net segmentation performance of the calcification and stent masks with and without incorporating the clDice loss.

		D_Pre	D_Rec	F1	β_0	β_1	β_2	χ	Dice	HD	HD95
Calcif.	-	77.87	88.62	82.35	16.65	27.76	4.06	27.53	0.80	180.04	12.70
	+clDice	79.14	88.86	83.01	13.06	27.34	4.18	28.59	0.82	175.39	6.58
Stents	-	64.75	82.10	64.56	7.60	85.50	5.50	82.00	0.68	137.14	74.90
	+clDice	66.00	85.00	68.88	6.00	90.50	5.70	85.60	0.69	162.73	109.03

Table 3: Average artery diameter (mm) and ratio of calcified artery per branch

	Aorta	C. i.	E. i.	C. f.	S. f.	Popliteal	TPT	A. t.	P.t.	Fibular
Diameter	8.73	4.58	4.04	4.87	3.23	3.26	2.31	1.76	1.67	1.61
Ratio	0.07	0.25	0.20	0.15	0.12	0.06	0.15	0.12	0.06	0.09

3.2 Automatic segmentation of anomalies

We reported segmentation performance of calcifications and stents in Table 2. Incorporation of the clDice loss function improved performance across all detection, overlap, and topology metrics for both structures. Calcifications were segmented with a Dice score of 0.82 and an F1-score of 83%, while stents achieved a Dice score of 0.69 and an F1-score of 68.9%. Despite the manual annotation challenges, both structures were segmented with reasonable accuracy. These results are likely due to the use of the semi-automatic detection, reducing inter-annotator variability and providing consistent labels.

3.3 Retrieval of pathological features.

We extracted the average artery diameter using VesselVio [3] and the average ratio of calcified artery in each branch across the dataset (Table 3). Additionally, 42% of the labeled scans have stents. Among them, patients have on average 1.67 stents. It demonstrate how our framework enables localized quantification of arterial pathology, supporting automated disease scoring.

4 Conclusion

By bridging advanced neural architectures with the clinical context of PAD, this work aimed to provide clinicians with an automated tool for detailed vascular mapping from CTA scans to help in the pre-surgical planning and treatment decision. It fills a critical gap on the application of the whole lower-limb arterial tree with the recognition of its main branches, calcification plaques and stents, in the specific context of PAD. In future works, we would like to improve the detection of the smaller branches in the below-the-knee region and use the segmentation volumes to automatically detect stenosis and thrombosis lesions.

Prospect of application. This method can be deployed in clinical workflows to support fast, consistent and personalized pre-surgical planning for PAD. It enables objective extraction of arterial features in each branch such as diameters, tortuosity, calcification burden, and stents from CTA scans. The segmented volume could be used for scoring systems to help PAD preoperative management.

Acknowledgments. This work has been supported by the French government, through the 3IA Côte d'Azur Investments in the Future project managed by the National Research Agency (ANR) with the reference number ANR-19-P3IA-0002. The authors are grateful to the OPAL infrastructure from Université Côte d'Azur.

Disclosure of Interests. The authors have no competing interests to declare that are relevant to the content of this article.

References

1. Anaya-Isaza, A., Mera-Jiménez, L., Zequera-Diaz, M.: An overview of deep learning in medical imaging. Informatics in Medicine Unlocked **26**, 100723 (2021)
2. Bagheri Rajeoni, A., Pederson, B., Clair, D.G., Lessner, S.M., Valafar, H.: Automated measurement of vascular calcification in femoral endarterectomy patients using deep learning. Diagnostics **13**(21), 3363 (2023)
3. Bumgarner, J.R., Nelson, R.J.: Open-source analysis and visualization of segmented vasculature datasets with vesselvio. Cell Reports Methods **2**(4), 100189 (2022)
4. Committee*, T.S., Jaff, M.R., White, C.J., Hiatt, W.R., Fowkes, G.R., Dormandy, J., Razavi, M., Reekers, J., Norgren, L.: An update on methods for revascularization and expansion of the tasc lesion classification to include below-the-knee arteries: a supplement to the inter-society consensus for the management of peripheral arterial disease (tasc ii). Journal of Endovascular Therapy **22**(5), 663–677 (2015)
5. Gerhard-Herman, M.D., Gornik, H.L., Barrett, C., Barshes, N.R., Corriere, M.A., Drachman, D.E., Fleisher, L.A., Fowkes, F.G.R., Hamburg, N.M., Kinlay, S., et al.: 2016 aha/acc guideline on the management of patients with lower extremity peripheral artery disease: a report of the american college of cardiology/american heart association task force on clinical practice guidelines. Journal of the American College of Cardiology **69**(11), e71–e126 (2017)
6. Hilbert, A., Rieger, J., Madai, V.I., Akay, E.M., Aydin, O.U., Behland, J., Khalil, A.A., Galinovic, I., Sobesky, J., Fiebach, J., et al.: Anatomical labeling of intracranial arteries with deep learning in patients with cerebrovascular disease. Frontiers in Neurology **13**, 1000914 (2022)
7. Hirsch, A.T., Criqui, M.H., Treat-Jacobson, D., Regensteiner, J.G., Creager, M.A., Olin, J.W., Krook, S.H., Hunninghake, D.B., Comerota, A.J., Walsh, M.E., et al.: Peripheral arterial disease detection, awareness, and treatment in primary care. Jama **286**(11), 1317–1324 (2001)
8. Hirsch, A.T., Haskal, Z.J., Hertzer, N.R., Bakal, C.W., Creager, M.A., Halperin, J.L., Hiratzka, L.F., Murphy, W.R., Olin, J.W., Puschett, J.B., et al.: Acc/aha guidelines for the management of patients with peripheral arterial disease (lower extremity, renal, mesenteric, and abdominal aortic). Journal of Vascular and Interventional Radiology **17**(9), 1383–1398 (2006)

9. Isensee, F., Jaeger, P.F., Kohl, S.A.A., Petersen, J., Maier-Hein, K.H.: nnU-Net: a self-configuring method for deep learning-based biomedical image segmentation. Nature Methods **18**(2), 203–211 (Feb 2021)
10. Kullo, I.J., Rooke, T.W.: Peripheral artery disease. New England Journal of Medicine **374**(9), 861–871 (2016)
11. Lareyre, F., Adam, C., Carrier, M., Raffort, J.: Automated segmentation of the human abdominal vascular system using a hybrid approach combining expert system and supervised deep learning. Journal of Clinical Medicine **10**(15), 3347 (2021)
12. Nordanstig, J., Behrendt, C.A., Baumgartner, I., Belch, J., Bäck, M., Fitridge, R., Hinchliffe, R., Lejay, A., Mills, J.L., Rother, U., et al.: Editor's choice–european society for vascular surgery (esvs) 2024 clinical practice guidelines on the management of asymptomatic lower limb peripheral arterial disease and intermittent claudication. European Journal of Vascular and Endovascular Surgery **67**(1), 9–96 (2024)
13. Norgren, L., Hiatt, W.R., Dormandy, J.A., Nehler, M.R., Harris, K.A., Fowkes, F.G.R., Group, T.I.W., et al.: Inter-society consensus for the management of peripheral arterial disease (tasc ii). Journal of vascular surgery **45**(1), S5–S67 (2007)
14. Ouyang, X., Gu, D., Li, X., Zhou, W., Chen, Q., Zhan, Y., Zhou, X.S., Shi, F., Xue, Z., Shen, D.: Towards a general computed tomography image segmentation model for anatomical structures and lesions. Communications Engineering **3**(1), 143 (2024)
15. Sermesant, M., Delingette, H., Cochet, H., Jais, P., Ayache, N.: Applications of artificial intelligence in cardiovascular imaging. Nature Reviews Cardiology **18**(8), 600–609 (2021)
16. Shit, S., Paetzold, J.C., Sekuboyina, A., Ezhov, I., Unger, A., Zhylka, A., Pluim, J.P., Bauer, U., Menze, B.H.: cldice-a novel topology-preserving loss function for tubular structure segmentation. In: Proceedings of the IEEE/CVF Conference on Computer Vision and Pattern Recognition. pp. 16560–16569 (2021)
17. Song, P., Rudan, D., Zhu, Y., Fowkes, F.J.I., Rahimi, K., Fowkes, F.G.R., Rudan, I.: Global, regional, and national prevalence and risk factors for peripheral artery disease in 2015: an updated systematic review and analysis. The Lancet Global Health **7**(8), e1020–e1030 (2019)
18. Wijnand, J.G., Zarkowsky, D., Wu, B., van Haelst, S.T., Vonken, E.J.P., Sorrentino, T.A., Pallister, Z., Chung, J., Mills, J.L., Teraa, M., et al.: The global limb anatomic staging system (glass) for clti: improving inter-observer agreement. Journal of Clinical Medicine **10**(16), 3454 (2021)
19. Yushkevich, P.A., Gao, Y., Gerig, G.: Itk-snap: An interactive tool for semi-automatic segmentation of multi-modality biomedical images. In: 2016 38th annual international conference of the IEEE engineering in medicine and biology society (EMBC). pp. 3342–3345. IEEE (2016)
20. Zhu, Y., Chen, L., Lu, W., Gong, Y., Wang, X.: The application of the nnu-net-based automatic segmentation model in assisting carotid artery stenosis and carotid atherosclerotic plaque evaluation. Frontiers in physiology **13**, 1057800 (2022)